Rock Mech Rock Eng (2014) 47:869–884
DOI 10.1007/s00603-012-0357-4

ORIGINAL PAPER

Modelling Discharge Rates and Ground Settlement Induced by Tunnel Excavation

G. Preisig · A. Dematteis · R. Torri · N. Monin · E. Milnes · P. Perrochet

Received: 29 June 2012 / Accepted: 13 December 2012 / Published online: 19 January 2013

Abstract Interception of aquifers by tunnel excavation results in water inflow and leads to drawdown of the water table which may induce ground settlement. In this work, analytical and numerical models are presented which specifically address these groundwater related processes in tunnel excavation. These developed models are compared and their performance as predictive tools is evaluated. Firstly, the water inflow in deep tunnels is treated. It is shown that introducing a reduction factor accounting for the effect of effective stress on hydrodynamic parameters avoids overestimation. This effect can be considered in numerical models using effective stress-dependent parameters. Then, quantification of ground settlement is addressed by a transient analytical solution. These solutions are then successfully applied to the data obtained during the excavation of the La Praz exploratory tunnel in the Western Alps (France), validating their usefulness as predictive tools.

Keywords Tunnel excavation · Flow rate · Ground settlement · Effective stress · Analytical and numerical modelling · La Praz

G. Preisig (✉) · E. Milnes · P. Perrochet
Centre for Hydrogeology and Geothermics, University of Neuchatel, Emile-Argand 11, 2000 Neuchâtel, Switzerland
e-mail: giona.preisig@unine.ch

A. Dematteis · R. Torri
SEA Consulting, Via Cernaia 27, 10121 Torino, Italy

N. Monin
Lyon Turin Ferroviaire (LTF), Avenue de la Boisse, BP 80631, 73006 Chambéry, France

List of Symbols

a (m)	Lateral spacing of the aquifer
b (1/m)	Coefficient characterising the elastic resistance of fractures to compression
C_v (1/m)	Aquifer compressibility
d (m)	Distance between the tunnel and the surface via the aquifer
e (m)	Aquifer thickness
E_s (Pa)	Aquifer elasticity
g (m/s^2)	Gravitational acceleration
h (m)	Pressure head
h_0 (m)	Pressure head prior to excavation
H (m)	Hydraulic head
H_0 (m)	Hydraulic head prior to excavation
K (m/s)	Hydraulic conductivity
K_0 (m/s)	Hydraulic conductivity at no stress
$\mathbf{K}$ (m/s)	Hydraulic conductivity tensor
L (m)	Tunnel/sector length
n (−)	Coefficient of asperities length statistical distribution
$\mathbf{n}$ (−)	Unit vector normal to the fracture plane
n_x, n_y, n_z (−)	Components of the unit normal vector
p (Pa)	Water pressure
Q (m^3/s)	Volumetric discharge rate
Q_0 (m^3/s)	Volumetric inflow rate without considering effective stress
Q_{red} (m^3/s)	Volumetric inflow rate considering effective stress
r (m)	Radial coordinate
r_0 (m)	Tunnel radius
s (m)	Water table drawdown
s_0 (m)	Drawdown at the tunnel
S_s (1/m)	Specific storage coefficient
S_{sm} (1/m)	Rock matrix specific storage coefficient
S_{sf} (1/m)	Fracture specific storage coefficient

S_{sf0} (1/m)	Fracture specific storage coefficient at no stress
t (s)	Time
T (m^2/s)	Transmissivity
v (m/s)	Excavation speed
x (m)	Spatial coordinate
z (m)	Elevation head
Z (m)	Depth
α (−)	Reduction factor
α_B (−)	Biot-Willis coefficient
ΔV_z (m)	Ground settlement
λ (−)	Ratio of horizontal to vertical stress
ν (−)	Poisson's ratio
ρ_w (kg/m^3)	Water density
ρ_r (kg/m^3)	Rock mass density
ϕ_0 (−)	Porosity at no stress
σ (Pa)	Stress
σ_h (Pa)	Horizontal stress
σ_v (Pa)	Vertical stress
σ' (Pa)	Effective stress
σ_0' (Pa)	Fracture closure effective stress

1 Introduction

Tunnel excavation modifies the natural hydrodynamic behaviour of groundwater systems. Under saturated conditions, tunnels behave as drainage structures causing drawdown of the water table. Depending on rock hydraulic conductivity, this may result in high flow rates into the underground excavation coupled with decreasing water pressures. Water inflow is a major cause which negatively affects tunnel progression, particularly when underestimated in the design phase. An example for this is shown in Fig. 1, where the cumulated tunnel discharge rate and excavation progression are presented as a function of time as well as the encountered geology. From 340 to 380 m the geology indicates a permeable sector of cargneules, mylonitic marbles and faults correlating with the first water inflow and the slowing down of excavation progression (Perrochet and Dematteis 2007). The highest water inflow occurred at the end of the permeable sector before the excavation speed increased again. From this point onward the cumulated tunnel discharge rate can no longer be directly correlated

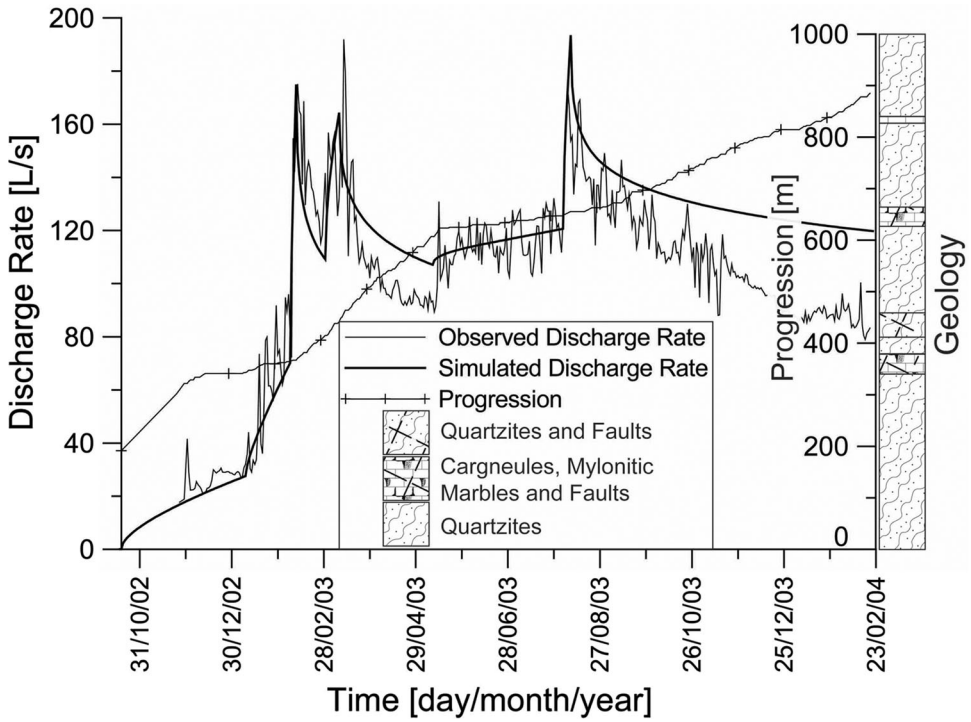

Fig. 1 Cumulated observed (*solid line*) and simulated (*solid bold line*) discharge rates and tunnel progression (*solid line with symbols*) as a function of time as well as the encountered geology, for the Modane/Villarodin–Bourget tunnel (exploratory adit for the basis tunnel of the Lyon-Turin railway project). From 340 to 380 m water inflow due to a permeable sector causes a significant slowing down of excavation progression between November 2002 and January–February 2003. For a detailed description of this case see Perrochet and Dematteis (2007)

with the excavation speed since the major part of water inflow occurs along an already excavated tunnel section.

Another issue of concern related to tunnel drainage are decreasing water pressures (water table decline) which may result in (1) the drying up of springs, and (2) ground settlement (aquifer consolidation) due to increased effective stress (Lombardi 1988; Zangerl et al. 2003; Perrochet 2005a, b; Perrochet and Dematteis 2007; Gargini et al. 2008).

As opposed to existing empirical approaches (Heuer 1995), two principal quantitative methods are used for the prediction of both discharge rates drained by the tunnel and drawdown. One method is based on numerical simulation (Anagnostou 1995; Molinero et al. 2002; Zangerl et al. 2003), while the other one is an analytical analysis (Goodman et al. 1965; Chisyaki 1984; El Tani 2003; Perrochet 2005a, b; Perrochet and Dematteis 2007).

Numerical simulations allow a detailed evaluation of the 3D evolution of the groundwater table with tunnel progression, but are computationally demanding and time consuming. Hence, in practice, hydrogeologists prefer analytical solutions for preliminary predictions and parametric sensitivity studies (Perrochet and Dematteis 2007). However, this latter approach is limited to specific flow configurations and boundary conditions, and requires significant hydrogeological simplifications. Moreover, the effect of effective stresses on parameters is neglected, which implies an overestimation of the flow rate drained by the underground excavation, especially for deep tunnels.

In non karstic alpine systems, as described by Bordet (1971), a tunnel excavated in fractured rock masses will first pass through a shallow and post-glacial decompression fractured slope with significant steady water inflow. Then, it will reach a deeper zone where steady water inflow is reduced by the increase of effective stress (closure of fractures) (Louis 1969), and by the decrease of fracture occurrence (Boutt et al. 2010). In both zones, but especially in the deeper zone, a tunnel intersecting a permeable saturated formation, will lead to a water inflow peak caused by a high initial hydraulic head, followed by a decreasing transient state.

The discharge rate and drawdown in the shallow zone after excavation will eventually become a function of the recharge regime (Gargini et al. 2008), as shown in Fig. 2 (sector 1). However, in the deep zone water inflow will either drop and reach steady state, if connected to a recharge body at the surface (such as a lake or a superficial quaternary aquifer), or will rapidly run dry, if not

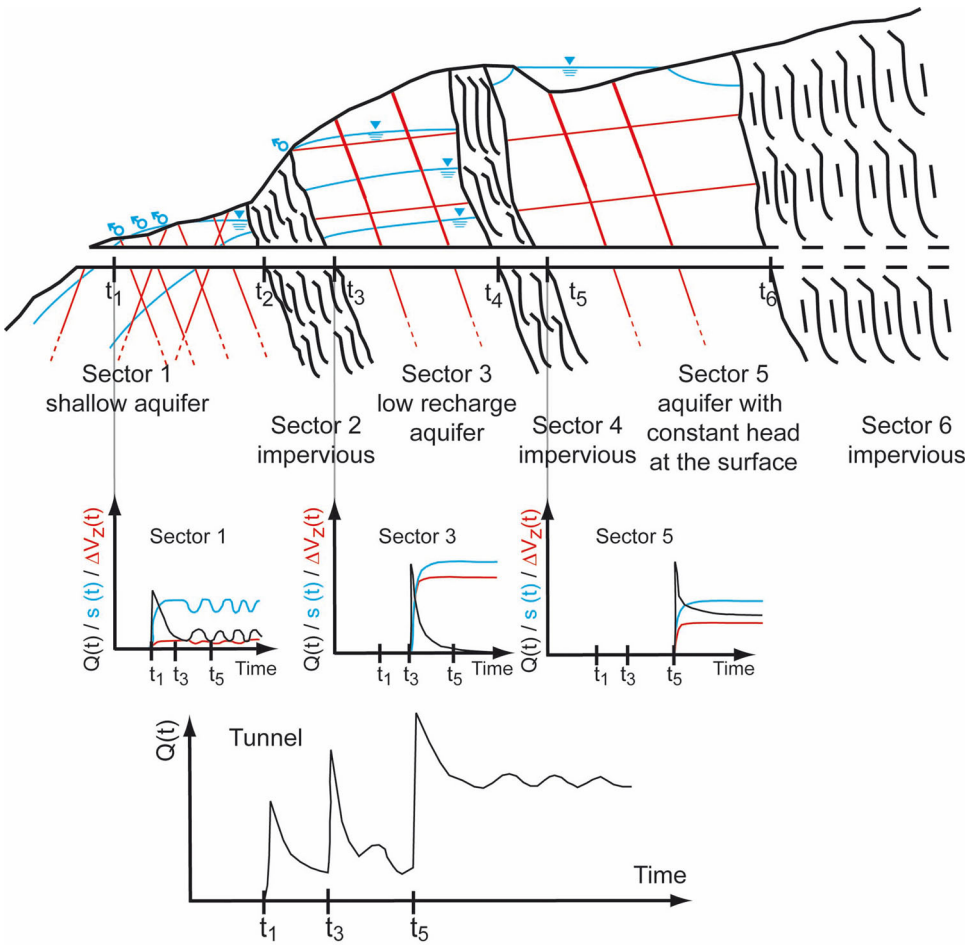

Fig. 2 *Schematic cross section* showing the main hydrogeological situations encountered during tunnel excavation into a typical alpine environment. Sector 1 is a shallow aquifer, after the initial transient depressurisation caused by tunnel excavation the discharge rate $Q(t)$ and the water table drawdown $s(t)$ become a function of recharge (rain and snow melt). Sector 3 is situated in the deep zone and is isolated from superficial recharge. The tunnel construction empties the system after strong initial water inflow, leading to complete water table decline and significant ground settlement $\Delta V_z(t)$. In sector 5, the presence of a lake at the surface provides substantial recharge rates that reduce aquifer depressurisation. Steady state water inflow will depend on the rock mass permeability and depth. Sectors 2, 4 and 6 are impervious (color figure online)

connected to a recharge zone. In the latter case, significant ground settlement may be observed on the surface due to the total water table decline (Lombardi 1988; Zangerl et al. 2003; Masset and Loew 2010; Preisig et al. 2012a). Due to the tunnel depth, it is very unlikely that a fluctuation of recharge on the surface will affect the inflow rate.

Figure 2 represents a conceptual model of a tunnel excavated in an alpine environment, illustrating the different situations described above.

The main aim of this work is to introduce a coupling of analytical solutions, pre-existing and newly developed ones, based on the conceptual model in Fig. 2, able to solve the drawdown, the drained discharge rate and the ground settlement caused by tunnel excavation, and to compare them with numerical methods. The impact of effective stress on discharge rates has been analysed by analytical and numerical analysis, leading to a reduction factor for equations solving the water inflow, in order to avoid overestimation.

This paper is divided in two sections: the first section presents analytical solutions and numerical methods specific to the modelling of the discharge rate, drawdown and ground settlement produced by tunnel excavation and proposes a reduction factor accounting for effective stress. The second section provides a field example.

2 Analytical and Numerical Methods

2.1 Analytical Solutions

There is a wide range of analytical formulas for solving the discharge rate drained by a tunnel. Goodman et al. (1965) presented a seminal steady state solution:

$$Q = \frac{2\pi K H_0 L}{\ln\left(\frac{2d}{r_0}\right)}, \tag{1}$$

where the symbols stand for hydraulic conductivity K, initial hydraulic head in tunnel H_0 (drawdown at the tunnel), tunnel depth d, tunnel length L, tunnel radius r_0 and discharge rate Q. If the tunnel is excavated through different geological zones, the total flow rate in the tunnel is obtained by the sum of each sector's discharge rate. Since then, other specific and practical formulas for the steady state case have been developed (Chisyaki 1984; El Tani 2003; Dematteis et al. 2005). For example, in Eq. (1) the assumption of an infinite aquifer can be removed by limiting the flow rate in the tunnel to a maximum corresponding to the local recharge, or by multiplying the flow rate in the tunnel with a factor considering the lateral extension of the permeable sector (Dematteis et al. 2005). Another possible improvement of Eq. (1) is to take into account the detailed geometry of the aquifer system, as shown in Fig. 3 (Dematteis et al. 2005):

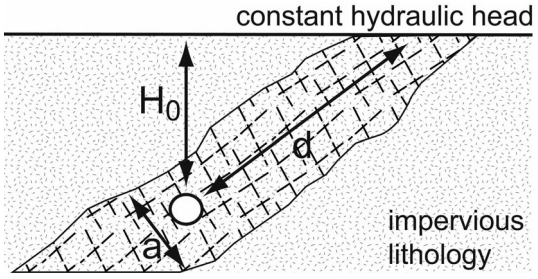

Fig. 3 *Schematic cross section* perpendicular to the tunnel axis showing the intersection between the tunnel and an inclined aquifer structure

$$Q = \frac{4\pi K H_0 L}{\ln\left(\frac{e^{\frac{4\pi d}{a}} + e^{\frac{-4\pi d}{a}} - 2}{e^{\frac{2\pi r_0}{a}} + e^{\frac{-2\pi r_0}{a}} - 2}\right)} = \frac{4\pi K H_0 L}{\ln\left(\frac{1-\cosh\left(\frac{4\pi d}{a}\right)}{1-\cosh\left(\frac{2\pi r_0}{a}\right)}\right)}, \tag{2}$$

where a is the lateral spacing of the aquifer system perpendicular to the distance d between the tunnel and the surface via the aquifer (Fig. 3). When d is vertical and a tends to infinity, Eq. (2) equals Eq. (1).

Concerning the transient state, Perrochet (2005a) proposed an analytical solution for the discharge rate produced during the excavation of a tunnel in an homogeneous formation, and subsequently expanded it to the heterogeneous case (Perrochet and Dematteis 2007):

$$Q(t) = 2\pi \sum_{i=1}^{N} \mathrm{H}(t - t_i) \times \int_0^{v_i(t-t_i)} \frac{K_i s_{0_i} \mathrm{H}(L_i - x)}{\ln\left[1 + \sqrt{\frac{\pi K_i}{S_{s_i} r_{0_i}^2}}\left(t - t_i - \frac{x}{v_i}\right)\right]} \mathrm{d}x, \tag{3}$$

where for each tunnel sector i, t is the time, t_i is the sector entry excavation time, H(u) is the Heaviside step-function, v_i is the excavation speed, s_{0_i} is the drawdown at the tunnel, L_i is the length over which the tunnel intersects the ith sector, x is the spatial coordinate along the tunnel axis with an origin at the entry of the permeable zone, and S_{s_i} is the specific storage coefficient. Using a geological oriented strategy of modelling, this transient solution reproduced satisfactorily the flow rate curve produced by the driving of the Modane/Villarodin–Bourget exploratory adit (Fig. 1), which was excavated by drill and blast.

In general, analytical formulas solving for the flow rate in a tunnel (Goodman et al. 1965; Chisyaki 1984; El Tani 2003; Perrochet 2005a; Perrochet and Dematteis 2007) are accurate and rapidly provide first estimations and sensitivity analysis. However, these formulas neglect the dependency of permeability on effective stress and tend to overestimation when depths/effective stress become significant. To avoid overestimation, one approach consists in

multiplying the calculated flow rates in a tunnel with a reduction factor, considering the dependency of hydraulic conductivity on effective stress.

2.1.1 Effective Stress Consideration for Deep Tunnels

Karl Terzaghi (1923) revealed that at a given depth, the effective stress state of a geological saturated material results from the total stress state lowered by the fluid pressure (one-dimensional form):

$$\sigma'_{zz} = \sigma_{zz} - \alpha_B p, \tag{4}$$

where σ'_{zz} is the vertical effective stress, σ_{zz} is the vertical stress, α_B is the Biot-Willis coefficient and p is the fluid pressure. If the fluid is water, then $p = \rho_w g h$, where ρ_w is the water density, g is the gravitational acceleration and h is the pressure head.

Hydrogeological parameters, e.g., hydraulic conductivity, porosity and specific storage coefficient, depend on the effective stress. This has been clearly identified by laboratory tests (Louis 1969; Walsh 1981; Tsang and Witherspoon 1981; Durham 1997; Hopkins 2000), field tests (Cappa 2006; Schweisinger et al. 2009), field measurements (Lombardi 1988; Rutqvist and Stephansson 1996; Zangerl et al. 2003) and analytical developments (Kim and Parizek 1999; Preisig et al. 2012a). The increase in effective stress results in decreasing hydrogeological parameters. In fractured stiff rock masses, these relationships have a dominant elastic reversible behaviour (Hansmann et al. 2012), and are well approximated by mathematical functions of the exponential type (Louis 1969; Preisig et al. 2012a). In unconsolidated materials, especially in clays and silts, at high effective stresses these relationships become plastic and irreversible (Galloway and Burbey 2011).

From Eq. (4) it follows that a change in effective stress can result from (1) a variation in total stress and/or (2) a change in fluid pressure. Concerning underground excavations, an increase in total stress can occur with increasing depth, and a drop in water pressure occurs because of tunnel drainage. However, it is important to note that the increase in total stress with depth does not always occur, because, depending on the principal stress orientation, the water pressure conditions, the Poisson's ratio effect and the geometry of aquifer structures (fractures/faults orientation), significant hydraulic conductivities can be found even at great depths (Masset and Loew 2010).

This permeability dependency on effective stress can not be directly introduced in formulas for tunnel drainage, because the permeability varies differently at each point of the aquifer. However, a reduction factor can be estimated by means of analytical or numerical analysis, and used to correct the calculated water flow rate in a tunnel, thereby avoiding overestimation.

2.1.2 Analytical Reduction Factor

Perrochet (2004) developed an analytical reduction factor, based on the water pressure-dependent fracture hydraulic aperture of Louis (1969). By combining this latter model function with the classical cubic law, he obtained a pressure-dependent hydraulic conductivity $K(h)$:

$$K(h) = K_0 e^{-3b(h_0 - h)}, \tag{5}$$

where K_0 is the hydraulic conductivity prior to a change in pressure head h, h_0 is the initial pressure head state, and b is a coefficient characterising the elastic resistance of fractures to compression. This parameter is linked to the elastic rock modulus E_s by: $b = \rho_w g / \phi / E_s$, where ϕ is rock porosity.

Considering Eq. (5) results in the non-linear steady groundwater flow equation:

$$\nabla \cdot (K(h) \nabla H) = 0; \quad H = h + z, \tag{6}$$

where H is the hydraulic head and z is the elevation potential. The flow rate in a tunnel Q_{red} obtained with Eq. (6) can be compared to that obtained with the linear form of the groundwater flow equation Q_0:

$$Q_{red} = Q_0 \alpha, \tag{7}$$

where α is the reduction factor. For any geometry and boundary conditions, it was shown (Perrochet 2004) that the reduction factor can be derived directly from a Kirchhoff transform of Eq. (5) as:

$$\alpha = \frac{Q_{red}}{Q_0} = \frac{1 - e^{-3b(h_0 - h)}}{3b(h_0 - h)}. \tag{8}$$

For a tunnel with an initial pressure head of h_0 = 1,000 m and with b = 0.001 1/m, Eq. (8) yields a reduction factor of 0.32.

The major advantage of Eq. (8) is the development from sound analytical principles. The main limitation is the neglection of the role of total stress on hydraulic conductivity reduction.

2.1.3 Numerical Reduction Factor

By considering the model function relating effective stress to fracture permeability proposed by Preisig et al. (2012a) and introducing it in a numerical simulator, it is possible to simulate groundwater flow rates in a tunnel taking into account or not effective stress-dependent permeabilities. The reduction factor is then calculated by the relation: $\alpha = Q_{red}/Q_0$.

The elastic model proposed by Preisig et al. (2012a) is:

$$K = K_0 \left[1 - \left(\frac{\sigma'}{\sigma'_0} \right)^{\frac{1}{n}} \right]^3, \tag{9}$$

where K is the hydraulic conductivity, K_0 is the no stress hydraulic conductivity, σ'_0 is the fracture closure effective stress, and n is a coefficient. This coefficient can be related to the statistical distribution of the fracture asperities, described in detail in (Preisig et al. 2012a). For a fracture characterised by many large asperities: $1 < n < 3.1$, and for a fracture characterised by small asperities: $3.1 < n < 9$. Eq. (9) allows considering the principal stress acting on the compressed asperities, and the water pressure in the fracture porosity:

$$\sigma' = \boldsymbol{\sigma}\mathbf{n}\cdot\mathbf{n} - \alpha_B p, \quad \boldsymbol{\sigma} = \begin{bmatrix} \sigma_{zz}\lambda & 0 & 0 \\ 0 & \sigma_{zz}\lambda & 0 \\ 0 & 0 & \sigma_{zz} \end{bmatrix}, \qquad (10)$$
$$= \rho_r g Z(\lambda n_x^2 + \lambda n_y^2 + n_z^2) - \alpha_B \rho_w g h$$

where ρ_r is the rock mass density, n_x, n_y, n_z are the components of the unit vector $\mathbf{n}$ normal to the fracture plane, and Z is the depth. The λ coefficient is the ratio of horizontal to vertical stress: $\lambda = \sigma_h/\sigma_v$. For an isotropic elastic compressible rock and in the absence of tectonic, erosional or post-glacial stress, horizontal stresses are driven by vertical stress. In such a case, λ depends on the Poisson's ratio v: $\lambda = v/(1 - v)$.

Here follows a quantification example of the reduction factor for a tunnel excavated into a vertical fault zone.

Theoretically, a vertical fault filled with water can be able to support a horizontal stress having a closing behaviour. As stated above, in the absence of tectonic, erosional or post-glacial stresses, the horizontal stress $\sigma_h = \sigma_{xx} = \sigma_{yy}$ acting perpendicularly onto the fracture plane, results from the vertical stress (overburden) $\sigma_v = \sigma_{zz}$ multiplied by the λ coefficient:

$$\sigma_h = \sigma_{zz}\lambda = \sigma_{zz}\frac{v}{(1-v)}. \qquad (11)$$

In crystalline fractured rocks, v is of the order 0.25, which implies a λ of 0.33. If the pressure head h in the fracture equals the depth Z, it follows that water pressure equals the horizontal stress, because $\rho_w \approx \rho_r \lambda$, and effective stress is close to zero. This equilibrium state results in a vertical fault being open even at great depths (Fig. 4). A tunnel excavation through the fracture causes a sudden water pressure decrease, and consequently a rapid decrease of the fracture hydraulic conductivity and of the discharge rate into the underground structure.

To highlight the reduction of the flow rate in a tunnel, several finite element numerical simulations have been realised for a tunnel excavated into a vertical fault at different depths. The numerical simulations are performed with no effective stress-dependent hydraulic conductivities and with effective stress-dependent ones. The fault is discretised by a vertical section of 3,000 × 3,000 m^2, with a tunnel of 10 × 10 m^2. For the different simulations, the initial pressure head h in the tunnel (tunnel depth) varies from 300 to 2,700 m, at intervals of 300 m. A constant hydraulic head of $H = 3{,}000$ m is specified at the domain top, while lateral and bottom boundaries are impervious. Finally, a constant atmospheric pressure is assigned in the tunnel, with a hydraulic head H that matches the tunnel elevation z: $H = z = 3{,}000{-}Z$. The initial head in the fault is at hydrostatic conditions. The right part of Fig. 4

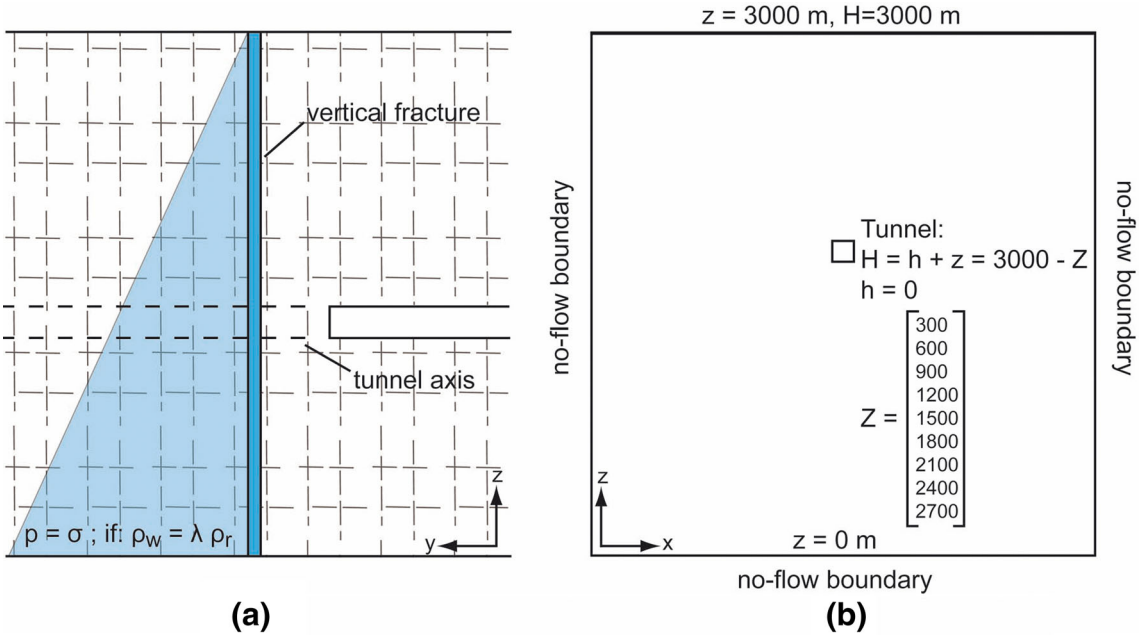

Fig. 4 Schematic cross sections **a** along the tunnel axis showing the water pressure state in the fracture, **b** perpendicular to the tunnel axis illustrating the geometrical configuration and the boundary conditions used in the numerical tests (color figure online)

summarises the boundary conditions and geometrical configurations used in the analysis.

The fracture presents a no stress hydraulic conductivity K_0 of 10^{-4} m/s, and the host rock is considered as an unaltered granite with standard values of: $\rho_r = 3000$ kg/m^3, $\sigma_0 = 3.5 \times 10^{10}$ Pa, and $n = 9$. In granitic rocks the λ coefficient generally matches 0.33, which implies the above explained initial equilibrium. For this analysis, three λ values are tested: $\lambda = 0.33$, $\lambda = 1.00$ (horizontal stresses correspond to the vertical ones), and $\lambda = 3.00$ (horizontal stresses are three times stronger than the vertical stress). The latter is possible in the presence of tectonic stresses or in areas that have been glaciated, such as in orogenic belts as measured in Mayeur and Fabre (1999). Note that, in the absence of horizontal stresses $\lambda = 0.00$, there is no effective stress reduction and the vertical fracture preserves a constant permeability, despite the water pressure decrease.

Simulations are carried out in steady and transient states. For the transient analysis the fracture effective stress-dependent specific storage coefficient proposed by Preisig et al. (2012a) is used:

$$\begin{aligned} S_s &= S_{sm} + S_{sf}; \\ S_{sf} &= S_{sf_0}\left[1 - \left(\frac{\sigma'}{\sigma'_0}\right)^{\frac{1}{n}}\right]; \end{aligned} \tag{12}$$

where the symbols stand for specific storage coefficient S_s, rock matrix specific storage coefficient S_{sm}, fracture specific storage coefficient S_{sf} and fracture specific storage coefficient S_{sf_0} under no stress conditions. In the analysis, S_s corresponds to 10^{-8} m^{-1} at no stress. Transient simulations are achieved with two types of boundary conditions on the domain surface: (1) constant atmospheric pressure ($H = z$), such as in the steady state case, and (2) no-flow condition. This latter condition implies the emptying of the fracture under tunnel drainage, as it happens when an underground excavation intersects an aquifer without a recharge zone or very weakly recharged.

2.1.4 Results and Discussion

As expected, flow rates in tunnels simulated with constant fault permeability are greater than those modelled with effective stress-dependent hydraulic conductivity, and increases with increasing initial pressure head at the tunnel location. On the contrary, with effective stress-dependent fracture hydraulic conductivity, the computed flow rate in the tunnel tends to stabilise despite increasing tunnel initial head (depth). This is due to the decrease of fracture permeability with the increase of effective stress caused by the tunnel drainage, and the subsequent fracture depressurisation and closure, especially for the case with horizontal stresses three times greater than vertical stress ($\lambda = 3$).

Figure 5 compares the simulated steady discharge rates into the tunnel, and shows the reduction coefficient $\alpha = Q_{\text{red}}/Q_0$ as a function of initial pressure head in the tunnel.

With λ equal to 0.33, the α coefficient varies from 0.32 for 300 m of initial head in the tunnel to 0.21 for 2,700 m of initial head in the tunnel, and the mean is 0.25. This slight decrease is due to the increase of horizontal stress with depth. These values correlate fairly well with the analytical reduction factor proposed by Perrochet (2004). With λ increasing from 1 to 3, the reduction factor decreases, due to the magnitude of horizontal stresses.

In the transient state, the reduction already starts when the excavation intersects the fracture. The value of the reduction is comparable to that obtained in the steady state and remains relatively constant during transient drainage. For the case with constant atmospheric pressure at the surface, simulated discharge rates and reduction factors stabilise to values calculated at steady state conditions. For the case with no flow conditions at the surface, the fracture is emptied. This total drainage is much slower with effective stress-dependent hydraulic conductivity.

The numerical analysis highlights the influence of principal stresses on the reduction factor. If stresses are negligible, the decrease in hydraulic conductivity depends only on the decrease in water pressures. In such a case, the value of the reduction factor is similar to those obtained with Eq. (8). When principal stresses become significant, the reduction coefficient decreases, especially in case of horizontal stresses greater than vertical stresses. The reduction coefficient also applies in transient conditions. Given its magnitude, this reduction should be considered in deep tunnels, beyond the post-glacial decompression shallow zone.

2.1.5 Coupling Discharge Rate in a Tunnel to Aquifer Consolidation

The consolidation of an aquifer intersected by a tunnel is a subtle process, especially in stiff rock masses. However, it can be detected by detailed geodetic measurements such as differential leveling, GPS or InSAR methods (Galloway and Burbey 2011). Despite the low magnitude of the phenomenon, a few tens of centimeters, differential consolidations can lead to very dangerous ground settlements. The abnormal behaviour of the Zeuzier arch dam (Switzerland) during the excavation of the Rawyl exploratory tunnel in 1978/1979 is a well known case study (Lombardi 1988; Schneider 1982).

The amount of ground settlement is directly linked to two principal parameters: (1) the compressibility of the aquifer and (2) the magnitude of the drawdown. Indirectly, it is also related to the flow rate in tunnel (Table 1).

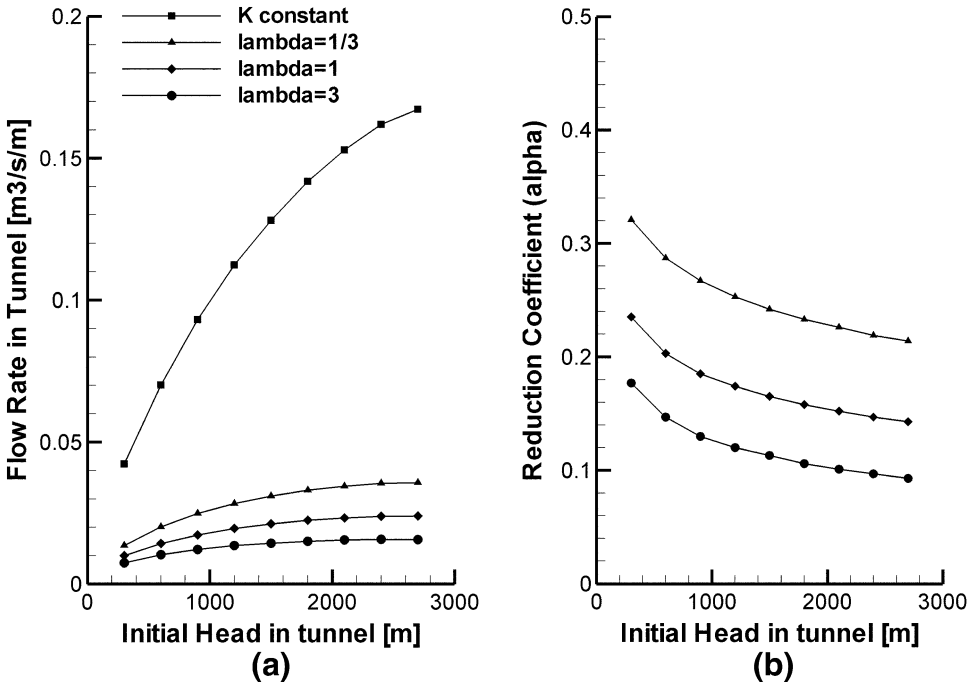

Fig. 5 **a** Simulated steady water flow rates in tunnel and **b** reduction coefficient as a function of initial pressure head in tunnel

Table 1 Maximum inflow, drawdown and ground settlement for different alpine tunnels

Tunnel	Flow Rate L/s	Drawdown m	Settlement cm	Geology	References
Gotthard Road Tunnel Switzerland	300	no data	12	Fractured crystalline rocks	Zangerl et al. (2003)
Rawyl Exploratory Adit Switzerland	>1000	230	12	Fractured meta-sedimentary calcareous schist	Schneider (1982), Lombardi (1988)
La Praz Exploratory Adit France	40	90	5	Fractured meta-sedimentary sandy schist	Dzikowski and Villemin (2009)
Modane/Villarodin-Bourget Exploratory Adit France	180	90	>3	Cargnieules, mylonitic marbles and faults	SOGREAH Consultants (2007), Lassiaz and Previtali (2007)
Loetschberg Railway Tunnel Switzerland	no data	60	19	Limestones and unconsolidated sediments	Vulliet et al. (2003)
Campo Valle Maggia Landslide drain Switzerland	no data	300	50	Fractured crystalline rocks and unconsolidated sediments	Bonzanigo (1999)

Using an alternative approach, Perrochet (2005b) suggests that the effect of drawdown $s(r, t)$ vanishes beyond a no-flow moving boundary located at the time-dependent radial distance $r = R(t)$:

$$s(r,t) = s_0\left(1 - \frac{2R(t)^2\ln(r/r_0) - r^2 + r_0^2}{2R(t)^2\ln(R(t)/r_0) - R(t)^2 + r_0^2}\right), \quad (13)$$

where the symbols stand for drawdown at the tunnel s_0, radial coordinate r and tunnel radius r_0. The no-flow moving boundary $R(t)$ is found to be (Barbosa 2009, Personal Communication):

$$R(t) = r_0\exp\left(\frac{\tan^{-1}(2\sqrt{\pi\alpha_t})}{\pi}\right)(1+\sqrt{\pi\alpha_t}), \quad (14)$$

where the dimensionless time α_t is:

$$\alpha_t = \frac{Tt}{Sr_0^2} \quad (15)$$

and where T is the transmissivity, t is the time, and S is the storage coefficient. A constant or a no-flow boundary can be added on Eq. (13) using the image method.

Considering Eq. (13) and integrating over the tunnel circumference, yields the tunnel discharge rate Q:

$$Q = 2\pi r_0\frac{\partial s(r,t)}{\partial r}|_{r=r_0} = \frac{2\pi T s_0}{\ln(1+\sqrt{\pi\alpha_t})}. \quad (16)$$

This latter equation constitutes the basis formula for the development of Eq. (3) (Perrochet and Dematteis 2007).

Using Eq. (13) and considering the classical aquifer-system consolidation theory proposed by Jacob (1940; 1950), a transient ground settlement $\Delta V_z(x,t)$ is obtained by expressing the drawdown in Cartesian coordinates (origin at the surface above the tunnel) and by a vertical integration of the drawdown cone (Fig. 6):

$$\begin{aligned}\Delta V_z(x,t) &= C_v s_0 \int_{z_b(x,t)=-s_0-\sqrt{R(t)^2-x^2}}^{z_t(x,t)=-s_0+\sqrt{R(t)^2-x^2}} s(x,z,t)\mathrm{d}z \\ &= -\frac{2}{3}C_v s_0 \sqrt{R(t)^2-x^2}\cdot \\ &\frac{\left(-4R(t)^2-2x^2-3r_0+3r_0{}^2-6R(t)^2 x\tan^{-1}\left(\frac{\sqrt{R(t)^2-x^2}}{x}\right)\frac{1}{\sqrt{R(t)^2-x^2}}\right)}{2R(t)^2\left(\ln\frac{R(t)}{r_0}-1\right)+r_0},\end{aligned} \quad (17)$$

where C_v is the aquifer compressibility expressed as: $C_v = \rho_w g/E_s$, E_s is the aquifer elasticity, and $z_t(x, t)$ and $z_b(x, t)$ are the top and the bottom elevation coordinates of the drawdown cone for the coordinate x and time t, respectively. Note that, for fractured rock masses the elasticity of water acting in fractures can be neglected because of the very low values of the rock mass porosity: in general <0.02. In such a case, the aquifer elasticity can be assumed equivalent to the rock elasticity. Eq. (17) computes the transient settlement in an infinite domain due to the tunnel drainage. In reality, aquifers are finite and the consolidation stops when the drawdown reaches the system boundaries. In such a case, the transient settlement of Eq. (17) must end when it reaches the maximum possible value $\Delta V_{z_{\max}}$:

$$\Delta V_{z_{\max}} = C_v s_0 e, \quad (18)$$

where e is aquifer thickness. Because of tunnel drainage, the horizontal strain can be obtained by a horizontal integration of Eq. (17) from the tunnel axis to the drawdown cone boundary, and taking into account the Poisson's ratio effect.

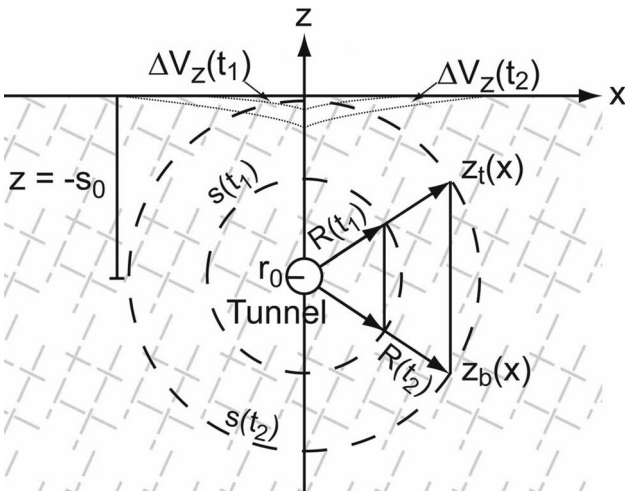

Fig. 6 Illustrative cross section perpendicular to the tunnel axis showing the temporal evolution of the drawdown cone (*dashed lines*). This aquifer depressurisation causes local deformations resulting in ground settlements (*dotted lines*)

2.2 Numerical Methods

A numerical groundwater flow model is a simplified version of: (1) a real aquifer, (2) the physical processes that take place within it, and (3) the aquifer's external solicitations (Bear and Cheng 2010). The tunnel excavation is the external solicitation. Below some generalities are discussed on the treatment of tunnels in 3D numerical simulations of groundwater flow and aquifer deformation.

As mentioned in Molinero et al. (2002), a tunnel can be introduced in a boundary value problem as a time-varying inner boundary. According to a time function describing the excavation progression, tunnel nodes become active as Dirichlet boundary conditions at constant atmospheric pressure (elevation head). This approach does not need the use of moving grids to simulate the advancing of the tunnel front, and consequently, it is not computationally demanding or time consuming, which is important in regional models. However, this method implies the presence of the tunnel as an inactive hole in the mesh since the start of the calculation.

For deep tunnels, effective stresses can be considered by combining stress-dependent functionals with the groundwater flow equation, as proposed by (Preisig et al. 2012a):

$$S_s(\sigma')\frac{\partial H}{\partial t} = \nabla\cdot(\mathbf{K}(\sigma')\nabla H); \quad H = h + z, \quad (19)$$

where $\mathbf{K}(\sigma')$ is the effective stress-dependent hydraulic conductivity tensor, and $S_s(\sigma')$ is the "storage" defined in Eq. (12).

The pressure head distributions resulting from the groundwater flow model can then be used to compute aquifer consolidation and ground subsidence. In this work, aquifer consolidation is computed following the modelling strategy proposed in (Preisig et al. 2012b).

3 Field Example: The La Praz Exploratory Tunnel

The La Praz exploratory tunnel is located in the French Western Alps (Maurienne Valley), and is part of the geological investigations undertaken by the Lyon-Turin railway project for the 57 km basis tunnel. From a tectonic

point of view, this exploratory adit is situated in the "Zone Houillère Briançonnaise", which in this area is composed of fractured meta-sedimentary sandy schist. The tunnel was entirely excavated in this formation by drill and blast (Fig. 7).

The first 900 m of the tunnel were excavated in the zone affected by post-glacial decompression, resulting in a permeable shallow fracture network (fractured sandy schists) (Dematteis et al. 2005). Then, the tunnel entered in the deeper zone of the mountain (unaltered sandy schists). The saturated zone was reached approximatively at a distance of 100 m from the tunnel portal. From this point, hydraulic heads before excavation increase because the tunnel gets deeper relative to both the topographic surface and the water table. The maximum tunnel depth and hydraulic head above the tunnel were 790–800 and 500 m, respectively. The average overburden (tunnel depth) is about 600 m (Fig. 7c).

During the excavation phase, the monitored data were the water inflow at the tunnel front, the total water inflow in the tunnel and the excavation progression. These data approximately cover the excavation period (1,100 days) corresponding to a progression of 2,500 m. Note that, the measure of total water inflow began only after the first water inflow. The monitoring network also includes several observation wells, geodetic points and springs (Fig. 7a, b).

The discharge rates in the tunnel indicate that the La Praz exploratory adit was excavated through an unconfined permeable shallow sector (decompression zone), before entering a deeper semipervious sector, where the rock mass permeability decreases because of (1) the diminution of fracture occurrence, and (2) the decrease of fracture permeability due to the increase of effective stress. Tunnel drainage caused an important water table drawdown, observed in wells. However, tunnel drainage did not completely empty the slope system, indicating active recharge from the nearby mountains. The water table decline resulted in a ground settlement of about 5 cm along the tunnel axis (Dzikowski and Villemin 2009).

3.1 Analytical Simulations

On the basis of the conceptual model presented above, and following the modelling strategy proposed in Perrochet and Dematteis (2007), the transient discharge rate drained during the excavation of the La Praz exploratory tunnel is

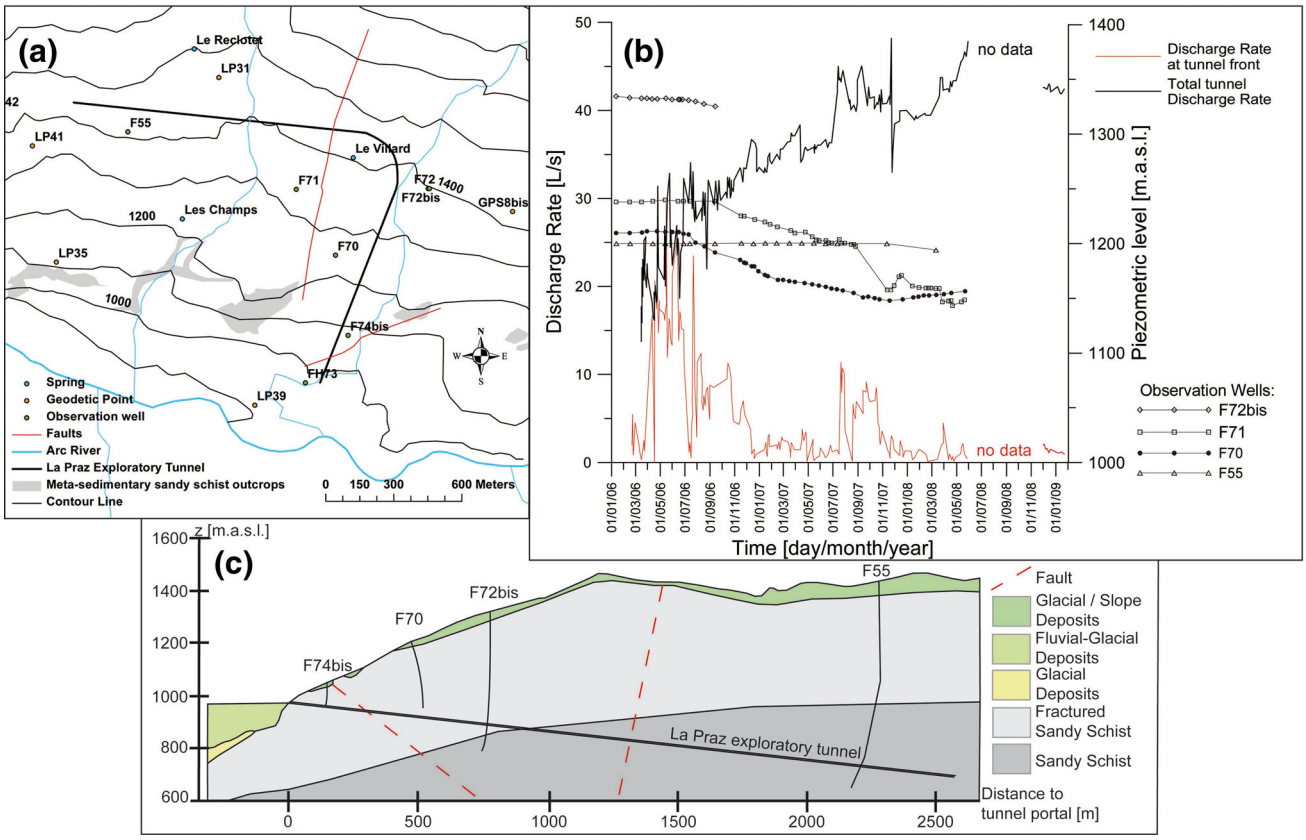

Fig. 7 **a** Map of the La Praz exploratory tunnel with observation wells, geodetic points and springs location (modified from Dzikowski and Villemin 2009). **b** Flow rate in tunnel, piezometric level as a function of time. **c** Cross section along the La Praz exploratory tunnel (modified from Ingénierie-ITM 2005) (color figure online)

simulated using Eq. (3). In a first model, the tunnel is separated into three sectors: an unsaturated sector, a saturated permeable sector representing the fractured sandy schists and a saturated semipervious sector representing the unaltered sandy schists. Sector lengths are estimated from the cross section of Fig. 7c, the excavation times are provided (green line of Fig. 7b), allowing to calculate the excavation speed for each sector.

In a second model, the tunnel is also separated into three principal zones according to the geology, but each zone is refined in order to correctly simulate the observed peaks (total of 16 sectors). The drawdown at the tunnel is estimated from the tunnel depth and the piezometric level measured at the observation wells. The analytical formula, Eq. (3), is calibrated using the measured water flow rates in the La Praz tunnel, by varying the hydraulic conductivity and the specific storage coefficient (Table 2; Fig. 8a).

The calibrated hydraulic conductivities are then introduced into Eq. (2) in order to compute the steady water flow rate in tunnel (with $H_0 = d$, $a \to \infty$). From an initial head in the tunnel greater than 100 m, the calculated steady discharge rates are multiplied with the reduction factors calculated with Eq. (8) ($b = 0.001$), or with those estimated from Fig. 5b for $\lambda = 0.33$ (Table 2). The tunnel radius is 4.5 m.

The water table drawdown and the ground settlement are simulated using Eqs. (13), and (17) for a cross section perpendicular to the tunnel axis at the penetration distance of 900 m. This distance corresponds to the contact between the weathered and the unaltered sandy schist. The available data of two observation points can be used for the calibration: the observation well **F71** and the geodetic point **GPS8bis** (Fig. 7a). For the settlement problem, only the consolidation of the fractured zone is considered. In such a case, the aquifer thickness in Eq. (18) corresponds to the thickness of the weathered sandy schist. The results of the analytical drawdown and ground settlement are presented in Fig. 8b, and the parametric values are shown in Table 3.

3.1.1 Discussion

The formulas used in the analysis rapidly and correctly reproduce the discharge rate, drawdown and ground

Table 2 Parametric values used in transient and steady calculations of the groundwater inflows, and results

Sectors	Geology	L_i [m]	t_i [d]	t_{i+1} [d]	v_i[m/d]	$s_i = H_{0_i}$ [m]	K_i [m/s]	S_i [1/m]	$Q_{\text{Eq. (2)}}$ [L/s]	$\alpha_{\text{Eq. (8)}}$	Q_{red1}	$\alpha_{\text{Fig. 5}b}$	Q_{red2}
Model 1: hydrogeological units													
1	Unsaturated zone	104	0	35	3.0	0	10^{-7}	5×10^{-4}	0.0	1.00	0.0	1.00	0.0
2	Fractured sandy schist	875ra>	35	537	2.0	220	10^{-7}	5×10^{-4}	26.4	0.73	19.3	0.39	10.3
3	Unaltered sandy schist	1,521	168	1,100	2.7	550	5×10^{-8}	1×10^{-5}	4.8	0.49	2.3	0.29	1.4
								$\sum$	31.2		21.6		11.7
Model 2: refined hydrogeological units													
1	Unsaturated zone	104	0	36	2.9	0	1×10^{-5}	5×10^{-3}	0.0	1.00	0.0	1.00	0.0
2	Fractured sandy schist	16	36	67	0.5	60	1×10^{-5}	5×10^{-3}	18.4	1.00	18.4	1.00	18.4
3		16	67	96	0.6	60	1×10^{-8}	1×10^{-3}	0.0	1.00	0.0	1.00	0.0
4		7	96	98	3.5	80	5×10^{-6}	1×10^{-3}	4.9	1.00	4.9	1.00	4.9
5		12	98	119	0.6	80	1×10^{-8}	1×10^{-3}	0.0	1.00	0.0	1.00	0.0
6		8	119	127	1.0	85	5×10^{-6}	1×10^{-3}	5.9	1.00	5.9	1.00	5.9
7		113	127	152	4.5	85	1×10^{-8}	1×10^{-3}	0.2	1.00	0.2	1.00	0.2
8		32	152	166	2.3	150	1×10^{-6}	1×10^{-3}	7.2	0.81	5.8	0.45	3.2
9		43	166	196	1.4	150	1×10^{-8}	1×10^{-3}	0.1	0.81	0.1	0.45	0.0
10		622	196	532	1.9	300	1×10^{-8}	1×10^{-3}	2.4	0.66	1.6	0.32	0.8
11		6	532	537	1.2	400	1×10^{-6}	1×10^{-3}	2.9	0.58	1.7	0.31	0.9
12	Unaltered sandy schist	111	537	591	2.1	400	1×10^{-9}	1×10^{-3}	0.1	0.58	0.0	0.31	0.0
13		20	591	598	2.9	500	1×10^{-7}	1×10^{-4}	1.2	0.52	0.6	0.30	0.3
14		416	598	776	2.3	500	1×10^{-9}	1×10^{-3}	0.2	0.52	0.1	0.30	0.1
15		288	776	862	3.3	600	5×10^{-9}	1×10^{-3}	1.0	0.46	0.5	0.29	0.3
16		686	862	1100	2.9	600	1×10^{-10}	1×10^{-4}	0.0	0.46	0.0	0.29	0.0
								$\sum$	44.5		39.8		35.0

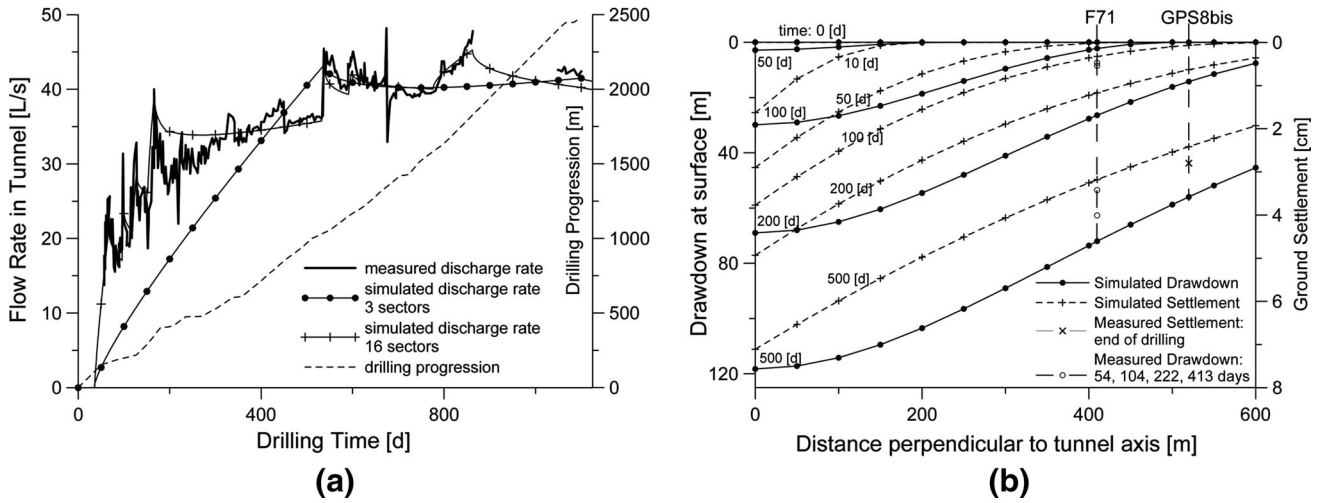

Fig. 8 **a** Comparison of measured water flow rates in tunnel (*bold line*) with analytical transient simulations: (1) hydrogeology oriented model of 3 sectors (*solid line with circles*) and (2) refined model of 16 sectors (*solid line with crosses*). **b** Simulated drawdown at the surface and ground settlement for a cross section perpendicular to the tunnel axis, at the tunnel distance of about 900 m. Note that: (1) the system is symmetric, and (2) the time is relative to the tunnel opening at 900 m

Table 3 Parametric values used in transient simulations of the drawdown and the ground settlement generated by the tunnel opening at the distance of 900 m

K (m/s)	S (1/m)	s (m)	E_s (Pa)	e (m)
1×10^{-5}	2×10^{-3}	400	1×10^{10}	400

settlement generated by the excavation of the La Praz exploratory tunnel.

As expected, the model 1 with three sectors is not able to accurately capture each flow rate pattern. However, this simple strategy allows good approximation of the general shape of the curve, and reproduces the essential features of the process. The detailed model can reproduce the observed flow spikes, but it is less coherent relative to its hydrodynamical parametrisation. In steady state calculations, the use of the reduction coefficient decreases the water inflow by a factor of 2 or 3, especially in deep sectors. The decrease is greater using the reduction coefficient in Fig. 5b, because, both the increase of total stress and the decrease of water pressure are taken into account. The use of this coefficient allows analytical formulas to be more realistic, in particular for deep tunnels. Unfortunately, due to the absence of long term field measurements, calculated steady flow rates cannot be compared with real observed values.

The analytical simulations of the drawdown and the ground settlement successfully reproduce the theoretical water table and ground surface depression cone induced by the opening of the tunnel (Fig. 8b). Moreover, the simulated values are in the same range of those observed in the field. A major disadvantage regarding the presented formulas is that they are constructed for an infinite domain. Also, in field applications, it is hard to define the aquifer boundaries, especially for the settlement problem. One approach consists in considering the base of the tunnel as the system bottom, neglecting the drawdown and the deformations below the tunnel.

3.2 Numerical Simulations

From the conceptual model presented above, a groundwater and a consolidation finite element model is constructed in order to reproduce the discharge rate, the water table decline and the ground settlement produced by the excavation of the La Praz exploratory tunnel. The 3D model discretisation respects the local topography and geology presented in Fig. 7 (Fig. 9). The before-mentioned conceptualisation of the rock mass, i.e., a permeable shallow sector, and a deeper semipervious sector, is reproduced using a contrast of hydraulic conductivities. As measured in Mayeur and Fabre (1999) for the North slope of the Arc Valley, vertical stresses correspond to the weight of the overburden. Both principal horizontal stresses are set 1.5 times higher than the vertical stresses; this condition applies well to orogenic and formerly glaciated areas, such as the Alps.

As reported earlier, groundwater flow occurs from the upstream area of the mountain slope towards the valley bottom. To reproduce the initial shape of the water table (before tunnel excavation), a steady state groundwater flow model is realised by specifying constant hydraulic heads along the upstream and downstream boundaries of the

model, approximately matching the topographic elevation (Fig. 9a). The model is calibrated using the pre-tunnel measured hydraulic heads, by varying the components of the hydraulic conductivity tensor (Table 4).

Tunnel excavation is then modelled. The tunnel is discretised as a cylinder of radius 4.5 m, following the trace shown in Fig. 7, and representing an inactivated hole in the mesh at the initial state. The excavation progression is simulated according to the recorded excavation data of Fig. 7b, by successively activating tunnel nodes as atmospheric Dirichlet boundaries (Fig. 9b). The calibrated hydraulic conductivity, and the hydraulic heads calculated

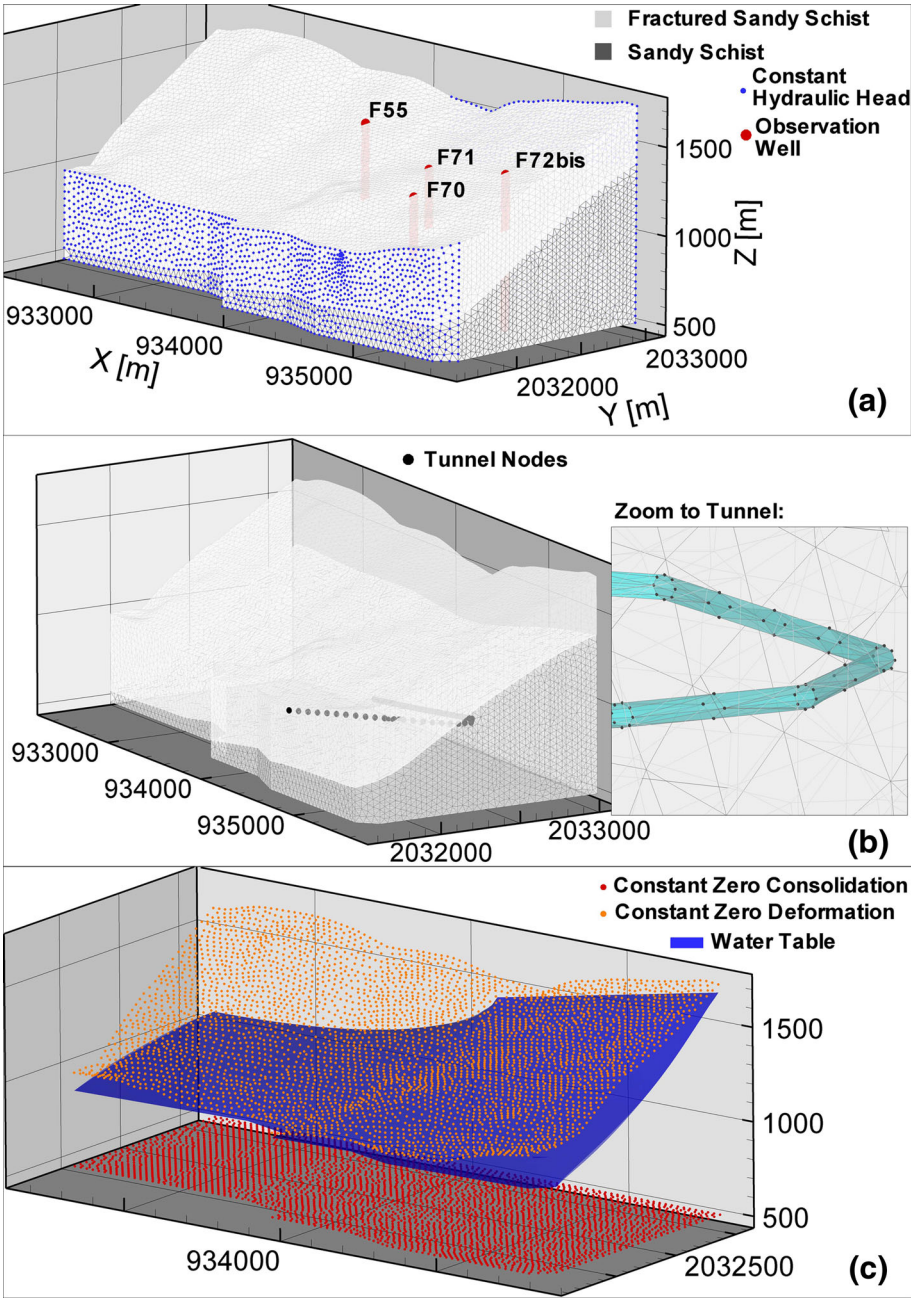

Fig. 9 3D model geometry showing **a** local geology, boundary conditions and observation wells for the steady state groundwater flow model, **b** the discretisation of the La Praz exploratory adit used in the transient model with a zoom to a part of the tunnel, and **c** boundary conditions and piezometric water levels for the consolidation simulation (color figure online)

Table 4 Parametric and geologic information used in the numerical models

Geology	$K_{0_{xx}}$ (m/s)	$K_{0_{yy}}$ (m/s)	$K_{0_{zz}}$ (m/s)	S_{s_0} (1/m)	ϕ_0	σ_0 (Pa)	λ	n
Weathered sandy schist	2×10^{-5}	1×10^{-5}	1×10^{-5}	1×10^{-4}	0.05	5×10^{8}	1.5	9
Unaltered sandy schist	2×10^{-7}	1×10^{-7}	1×10^{-7}	1×10^{-4}	0.005	5×10^{8}	1.5	9

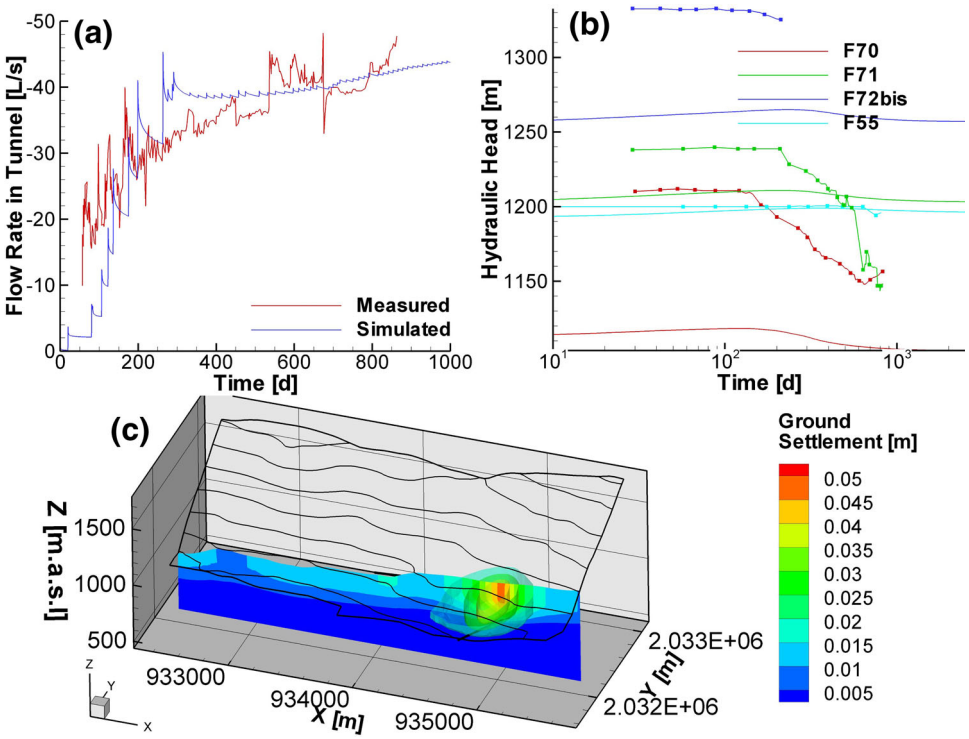

Fig. 10 Comparison of **a** measured water flow rates in tunnel (*red line*) with simulated values (*blue line*), and **b** measured drawdown in observation wells (*solid lines with dots*) with simulated ones (*solid lines*). **c** Simulated bulbs and cross section of ground settlement with the La Praz tunnel trajectory and the local topography (color figure online)

with the steady state model before tunnel excavation, are introduced as input. In this transient analysis, hydrogeological parameters are considered as stress-dependent. The temporal evolution of the simulated inflows and water table drawdown can be seen in Fig. 10.

Finally, the rock mass consolidation, ground settlement, caused by the tunnel drainage is computed using the simulated pressure head distributions before and after tunnel perturbation (Fig. 9c). The problem is solved using the deformation equations proposed by Preisig et al. (2012a, b), based on the assumptions that aquifers deform elastically, the principal stresses do not change with water depletion and the consolidation only results from fractures porosity closure. The calibrated parameters are shown in Table 4, where ϕ_0 is the no stress porosity of the rock mass.

The detailed 3D finite element model of Fig. 9 respecting the topography and geology of the La Praz area, and the 3D tunnel trajectory was constructed and generated using the mesh generator software `GMSH` (Geuzaine and Remacle 2009). The groundwater flow and rock consolidation models were computed using the multipurpose `Ground Water (GW)` finite element software (Cornaton 2007).

3.2.1 Discussion

Groundwater inflow in tunnel and the ground settlement are well reproduced by the numerical analysis (Fig. 10a, c). On the contrary, at observation wells, simulated hydraulic heads and drawdowns do not satisfactorily reproduce the observed values (Fig. 10b). This is due to the upstream hydraulic boundary condition used in the model, which is considered to be constant. In reality the upstream hydraulic heads have also to be modified with time and excavation progression.

As anticipated, the numerical analysis has been time consuming, especially during (1) the discretisation of the tunnel in the 3D finite element mesh, and (2) the calibration phase.

4 Conclusion

This work has focused on quantitative tools specific to the problem of groundwater inflow and related mechanisms during and after tunnel excavation. Three major hydrogeological issues are related to tunneling: (1) transient and steady inflow rates in tunnels due to the drainage of surrounding aquifers, (2) water table decline leading to the drying up of springs, and (3) consolidation of the aquifer (related to the water table decline) leading to ground settlement. All of these processes can be correctly reproduced by analytical solutions or by numerical simulation.

It has been shown that both approaches capture the main hydrogeological processes, and can be used as predictive tools. However, in practice, the use of numerical models is limited because (1) the method is time consuming and (2) of the difficulty to introduce tunnels in large scale, geologically oriented 3D meshes. Moreover, at a regional scale 3D geological models usually have a low reliability.

Analytical formulas require simplifications of aquifer structures and of the groundwater flow system, but are able to reproduce the governing mechanisms. Based on the geological and hydrogeological information along and perpendicular to the tunnel axis, the presented analytical solutions lead to rapid first estimations of the transient and steady discharge rates produced by a tunnel, as well as of water table decline and associated ground settlement, as demonstrated in the La Praz field example. The reduction factor allows overall consideration of the impact of effective stress on hydrogeological parameters, in particular on hydraulic conductivity, and improves the accuracy of standard equations. This factor should be used in the analysis of groundwater inflow in deep tunnels.

Acknowledgments This work was performed within the framework of the Lyon Turin Ferroviaire project (LTF), which provided the data observed in the field. The authors wish to thank LTF for the collaboration, and are particularly grateful to Nathalie Monin. Thanks are also to the anonymous reviewers for their constructive comments.

References

Anagnostou G (1995) The influence of tunnel excavation on the hydraulic head. Int J Numer Anal Methods in Geomech 19(10): 725–746

Bear J, Cheng AHD (2010) Modeling groundwater flow and contaminant transport. Springer, Berlin

Bonzanigo L (1999) Lo slittamento di Campo Vallemaggia. PhD thesis, Swiss Federal Institute of Technology Zürich

Bordet C (1971) L'eau dans les massifs rocheux fissurés. Observations dans les travaux souterrains. Tech rep, Université de Liége, BEL

Boutt D, Diggins P, Mabee S (2010) A field study (Massachusetts, USA) of the factors controlling the depth of groundwater flow systems in crystalline fractured-rock terrain. Hydrogeol J 18(8): 1839–1854

Cappa F (2006) Role of fluids in the hydromechanical behavior of heterogeneous fractured rocks: in situ characterization and numerical modelling. Bull Eng Geol Env 65:321–337

Chisyaki T (1984) A study of confined flow of ground water through a tunnel. Ground Water 22(2):162–167

Cornaton FJ (2007) Ground Water: a 3-D ground water and surface water flow, mass transport and heat transfer finite element simulator, reference manual. Centre for Hydrogeology and Geothermics, Neuchâtel

Dematteis A, Perrochet P, Thiery M (2005) Nouvelle liaison ferroviaire transalpine Lyon-Turin, Etudes hydrogéologiques 2002–2004. Tech rep, Lyon Turin Ferroviaire, Chambéry

Durham WB (1997) Laboratory observations of the hydraulic behavior of a permeable fracture from 3800 m depth in the KTB pilot hole. J Geophys Res 102:18405–18416

Dzikowski M, Villemin T (2009) Rapport d'expertise: hydrogéologie et géodésie de la descenderie de La Praz. Tech rep, Lyon Turin Ferroviaire (LTF), Chambery

El Tani M (2003) Circular tunnel in a semi-infinite aquifer. Tunn Undergr Space Tech 18(1):49–55

Galloway D, Burbey T (2011) Review: regional land subsidence accompanying groundwater extraction. Hydrogeol J 19(8): 1459–1486

Gargini A, Vincenzi V, Piccinini L, Zuppi G, Canuti P (2008) Groundwater flow systems in turbidites of the Northern Apennines (Italy): natural discharge and high speed railway tunnel drainage. Hydrogeol J 16(8):1577–1599

Geuzaine C, Remacle JF (2009) Gmsh: a three-dimensional finite element mesh generator with built-in pre- and post-processing facilities. Int J Numer Methods Eng 79(11):1309–1331

Goodman R, Moye D, Van Schaikwyk A, I J (1965) Ground water inflows during tunnel driving. Bull Int Assoc Eng Geol 2(1): 39–56

Hansmann J, Loew S, Evans K (2012) Reversible rock-slope deformations caused by cyclic water-table fluctuations in mountain slopes of the Central Alps, Switzerland. Hydrogeol J 20(1):73–91

Heuer R (1995) Estimating Rock Tunnel Water Inflow. In: Rapid Excavation and Tunneling Conference, San Francisco, June 18–21

Hopkins D (2000) The implications of joint deformation in analyzing the properties and behavior of fractured rock masses, underground excavations and faults. Int J Rock Mech Min Sci Geomech Abstr 37(1–2):175–202

Ingénierie-ITM (2005) Descenderie de La Praz: synthèse géologique, hydrogéologique et géotechnique. Tech rep, Lyon Turin Ferroviaire (LTF), Chambery

Jacob C (1940) On the flow of water in an elastic artesian aquifer. Am Geophys Union 21:574–586

Jacob C (1950) Flow of ground water. In: Rouse H (ed), Engineering hydraulics: Proceedings of the Fourth Hydraulics Conference, Iowa Institute of Hydraulic Research, Iowa City

Kim JM, Parizek R (1999) A Mathematical Model for the Hydraulic Properties of Deforming Porous Media. Ground Water 37(4): 546–554

Lassiaz P, Previtali I (2007) Descenderie et Galerie de reconnaissance de Modane/Villarodin—Bourget: Suivi et Auscultation Géodésique. Tech rep, Lyon Turin Ferroviaire, Chambéry

Lombardi G (1988) Les tassements exceptionnels au barrage de Zeuzier. Publ Swiss Soc Soil Rock Mech 118:39–47

Louis C (1969) A study of groundwater flow in jointed rock and its influence on the stability of rock masses. Tech rep 9, Rock Mech, Imperial College, London

Masset O, Loew S (2010) Hydraulic conductivity distribution in crystalline rocks, derived from inflows to tunnels and galleries in the Central Alps, Switzerland. Hydrogeol J 18(4):863–891

Mayeur B, Fabre D (1999) Measurement and modeling of natural stresses. Application to the Maurienn- Ambin tunnel project. Bull Eng Geol Env 58(1):45–59

Molinero J, Samper J, Juanes R (2002) Numerical modeling of the transient hydrogeological response produced by tunnel construction in fractured bedrocks. Eng Geol 64(4):369–386

Perrochet P (2004) Facteur de réduction des débits en tunnels profonds. Tech rep, Centre for Hydrogeol and Geotherm, University of Neuchâtel

Perrochet P (2005) Confined flow into a tunnel during progressive drilling: an analytical solution. Ground Water 43(6):943–946

Perrochet P (2005) A simple solution to tunnel or well discharge under constant drawdown. Hydrogeol J 13:886–888

Perrochet P, Dematteis A (2007) Modeling transient discharge into a tunnel drilled in a heterogeneus formation. Ground Water 45(6): 786–790

Preisig G, Cornaton F, Perrochet P (2012a) Regional flow simulation in fractured aquifers using stress-dependent parameters. Ground Water 50(3):376–385

Preisig G, Cornaton FJ, Perrochet P (2012b) Simulation of flow in fractured rocks using effective stress-dependent parameters and aquifer consolidation. In: Models—repositories of knowledge, MODELCARE 2011, vol 355. IAHS Publication, pp 273–279

Rutqvist J, Stephansson O (1996) A cyclic hydraulic jacking test to determine the in situ stress normal to a fracture. Int J Rock Mech Min Sci Geomech Abstr 33(7):695–711

Schneider T (1982) Geological Aspects of the Extraordinary Behaviour of Zeuzier Arch Dam. Wasser, Energie, Luft - Eau, Energie, Air 74(3):81–94

Schweisinger T, Svenson E, Murdoch L (2009) Introduction to hydromechanical well tests in fractured rock aquifers. Ground Water 47(1):69–79

SOGREAH Consultants (2007) Descenderie de Modane/Villarodin—Bourget: étude de faisabilité de reutilisation des eaux d'exhaure de la partie montante. Tech rep, Lyon Turin Ferroviaire (LTF), Chambery

Terzaghi K (1923) Die berechnung der durchlässigkeitziffer des tones aus dem verlauf der hydrodynamischen spannungserscheinungen. Akad Wissensch Wien Sitzungsber Mathnaturwissensch Klasse IIa 142(3-4):125–138

Tsang Y, Witherspoon P (1981) Hydromechanical behavior of a deformable rock fracture subject to normal stress. J Geophys Res 86(B10):9287–9298

Vulliet L, Koelbl O, Parriaux A, Védy JC (2003) Gutachtenbericht über die Setzungen von St. German, in Auftrag der BLS Alptransit AG. Tech rep

Walsh JB (1981) Effect of pore pressure and confining pressure on fracture permeability. Int J Rock Mech Min Sci Geomech Abstr 18:429–435

Zangerl C, Eberhardt E, Loew S (2003) Ground settlements above tunnels in fractured crystalline rock: numerical analysis of coupled hydromechanical mechanisms. Hydrogeol J 11:162–173